

# Laboratory exercise for the radiometry student

Michael A. Marciniak\*

Air Force Institute of Technology, Department of Engineering Physics,  
Wright-Patterson Air Force Base, Ohio, United States

---

**ABSTRACT.** The U.S. Air and Space Forces require optical expertise among their personnel. The Air Force Institute of Technology offers a graduate optics curriculum, which includes a three-course sequence to educate students in the optical concepts of radiometry and radiometric instrumentation. We find radiometry is often a deceptively difficult concept for students to master. To address this, we have developed an experiment in our optics-laboratory coursework to help them gain this mastery. A Fourier-transform infrared spectrometer (FTS) is used to collect spectral data from an unknown sample. FTS calibration and data collection are discussed here, as are the two specific samples used, one with specular reflectance properties, the other with diffuse. The analysis methodology used on the data is also discussed. This is a good radiometry exercise to reveal to the student what can be learned about an unknown material's optical properties in a remote-sensing scenario and is the basis upon which the limiting simplifications of this initial experiment may be generalized to address more difficult, but more realistic, remote-sensing analyses.

© The Authors. Published by SPIE under a Creative Commons Attribution 4.0 International License. Distribution or reproduction of this work in whole or in part requires full attribution of the original publication, including its DOI. [DOI: [10.1117/1.OE.63.7.071405](https://doi.org/10.1117/1.OE.63.7.071405)]

**Keywords:** radiometry; radiometric data collection; infrared laboratory; bidirectional reflectance distribution function; radiance

Paper 20231120SS received Nov. 28, 2023; revised Jan. 30, 2024; accepted Feb. 9, 2024; published Mar. 6, 2024.

---

## 1 Introduction

The Graduate School of Engineering and Management at the Air Force Institute of Technology (AFIT) educates military and civilian students from the U.S. Air and Space Forces (USAF/USSF), Department of Defense, other government agencies, international partners, and government contractors, providing academic programs with a defense-related focus and research on high-priority defense problems.<sup>1</sup> There is a clear need for optical expertise in USAF applications, ranging from active systems, such as laser range-finding and radar, to passive systems, such as imaging-, spectral-, and polarimetric-remote sensing. This paper introduces an experiment, which is centered on radiometry and radiometric instrumentation, from the laboratory portion of our optics curriculum.

Radiometry is the measurement of a radiometric quantity, e.g., irradiance or incident power/unit area on a surface, often with the goal of determining another radiometric quantity of a distant source, e.g., its intensity (power/unit solid angle into which that radiation flows) or its radiance (radiating power/unit area of a surface/unit solid angle into which the radiation flows), which is not otherwise accessible. Broadly, a radiometer is an apparatus for quantifying some property of incident radiation. The receiving aperture of a radiometer is used as the reference position for the incident radiation, with the assumption that the radiation would affect any other instrument similarly placed. Calculation of the desired radiometric quantity at the remote location using the values determined at the radiometer's aperture requires additional information, such as

---

\*Address all correspondence to Michael A. Marciniak, [michael.marciniak@us.af.mil](mailto:michael.marciniak@us.af.mil)

knowledge of the intervening atmosphere or the distance to the source, etc. The challenge of radiometry is in understanding how these all affect the radiometer's output.<sup>2</sup>

Radiometric theory appears to be simply geometric and phenomenological, but Wolf established the relationship between it and the modern theories of radiation, such as Maxwell's electromagnetic theory and the quantum theory of radiation.<sup>3</sup> When the optics student assumes radiometry is simply geometric, its nuances often become deceptively difficult for them to understand; e.g., the basic quantity in radiometry is radiance,  $L$

$$L \triangleq \frac{\partial^2 \Phi}{\partial A_{s\perp} \cos \theta_s \partial \Omega_s} (\text{W cm}^{-2} \text{ Sr}^{-1}), \quad (1)$$

where  $\Phi$  is the power or joule flux (W),  $A_{s\perp}$  is the emitting area of the source ( $\text{cm}^2$ ),  $\theta_s$  is the planar angle between the source's surface normal and the direction of propagation of the radiation, and  $\Omega_s$  is the solid angle into which the radiation flows (Sr). Integrating both sides of Eq. (1)

$$\Phi = \int \int L \cos \theta_s dA_{s\perp} d\Omega_s = \int \int \int L \cos \theta_s \sin \theta_s dA_{s\perp} d\theta_s d\phi_s (\text{W}), \quad (2)$$

where  $(\theta_s, \phi_s)$  put  $\Omega_s$  in spherical coordinates, where  $\theta_s$  is the declination angle relative to the surface normal and  $\phi_s$  is the azimuthal angle about the surface normal. The common "small-angle approximation" to Eq. (2) is valid when  $L$  is independent of  $(\theta_s, \phi_s)$  over their bounds of integration, and it eliminates the need to integrate over  $\Omega_s$  in Eq. (2). But students often fail to recognize this as the reason for the approximation and focus on a particular size of  $\Omega_s$  at which they will not have to integrate. Furthermore,  $A_{s\perp} \cos \theta_s$ , the projected area of the source, still applies in the small-angle case, but students often think a "small-angle approximation" also eliminates the need for the  $\cos \theta_s$  term. They fail to recognize that intensity,  $I$

$$I \triangleq \frac{\partial \Phi}{\partial \Omega_s} = \int L \cos \theta_s dA_{s\perp} (\text{W Sr}^{-1}), \quad (3)$$

is the ultimate small-angle case, in which the projected area of the source is maintained. And even though using intensity implies considering the source as a point source, to do the calculations correctly, the projected area of the actual source must be considered.

At AFIT, we offer a three-course sequence, essentially in applied radiometry. "Optical radiometry and detection" develops the terminology of radiation transfer and measurement, as well as an understanding of optical detection. "Infrared (IR) Technology" presents the principles required for the analysis of electro-optic systems, with emphasis on those systems operating in the IR, and is often where the AFIT student finally masters the radiometric concepts. And "Electro-Optical Systems Lab" is a laboratory-and-lecture course that introduces laboratory techniques for the measurement of optical observables, i.e., emissions and reflections of optical radiation from targets.<sup>4</sup> This paper will focus on a particular radiometry experiment developed to reassert and clarify the radiometric concepts and approximations for the students in our Electro-Optical-Systems-Lab course.

The bidirectional reflectance distribution function (BRDF) radiometrically describes reflections from a surface as the ratio of the radiance ( $L_r$ ) reflected from a surface into a small solid angle in a given direction in spherical coordinates with respect to the surface normal  $(\theta_r, \phi_r)$ , to the incident irradiance ( $E_i$ ) from a given direction  $(\theta_i, \phi_i)$ <sup>5</sup>

$$\text{BRDF}(\theta_i, \phi_i, \theta_r, \phi_r) \triangleq \frac{dL_r(\theta_r, \phi_r)}{dE_i(\theta_i, \phi_i)} (\text{Sr}^{-1}). \quad (4)$$

Although the BRDF is introduced in our optical-radiometry-and-detection text,<sup>6</sup> we develop it much further in our IR-Technology course. Just as Wolf tied the phenomenological radiometry to modern optical theories, Greffet and Nieto-Vesperinas also derived the radiometric BRDF in terms of modern electromagnetic theory.<sup>7</sup>

We also introduce the scene rendering equation, often used in computer graphics and which uses the BRDF, in our IR-Technology course<sup>8,9</sup>

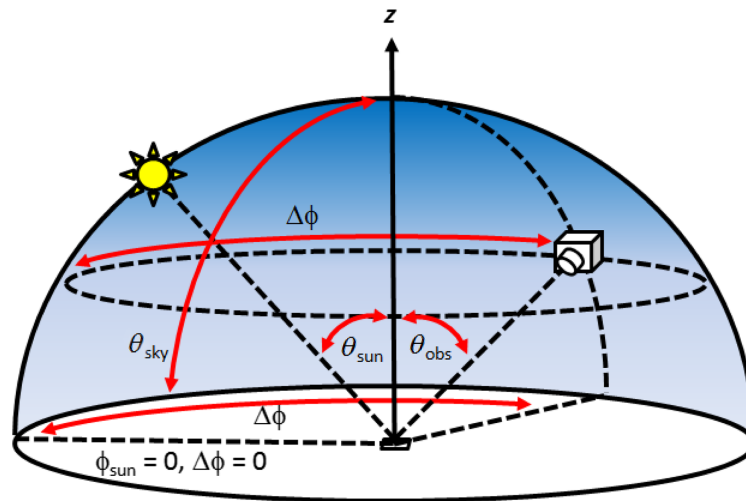


**Fig. 1** Classroom remote-sensing scenario introduced in AFIT’s IR-Technology course. An observed surface is located at the center of the spherical coordinate system shown. It is illuminated by the entire hemisphere above it with declination angles,  $0 \leq \theta_{\text{sky}} \leq \pi/2$ , and assumed to be symmetric azimuthally. It is illuminated by a source that subtends a small solid angle at position  $(\theta_{\text{sun}}, \phi_{\text{sun}} = 0)$ . It is observed from position is  $(\theta_{\text{obs}}, \Delta\phi)$ .

$$L_s(\Omega_r, \lambda) = L_e(\Omega_r, \lambda) + \int_{2\pi} \text{BRDF}(\Omega_i, \Omega_r) L_i(\Omega_i, \lambda) \cos \theta_i d\Omega_i, \quad (5)$$

where  $L_s$  is the spectral radiance of a surface and is the sum of the self-emitted spectral radiance,  $L_e$ , and the reflected spectral radiance (the BRDF integral);  $\Omega_r$  and  $\Omega_i$  are the reflected and incident solid angles, respectively;  $\lambda$  is wavelength;  $L_i$  is the radiance incident on the surface; and  $\theta_i$  is again the incident declination angle with respect to the surface normal. Strictly,  $\text{BRDF}(\theta_i, \phi_i, \theta_r, \phi_r)$  is the “bidirectional” case, which cannot be measured, and  $\text{BRDF}(\Omega_i, \Omega_r)$  describes a “bi-conical” case, which can be.<sup>10</sup> However, the solid angles,  $(\Omega_i, \Omega_r)$ , are typically small enough to be considered bidirectional—this experiment will show that to the student.

We also introduce the scenario shown in Fig. 1 in our IR-Technology course as a tractable case in which the signature contributions from both self-emission and reflection of an observed surface, here at the center of the spherical coordinate system shown, may be computed using the rendering equation. The surface is illuminated by the entire hemisphere above the surface, e.g., it could be the sky with declination angles,  $0 \leq \theta_{\text{sky}} \leq \pi/2$ , and which we assume is azimuthally symmetric to keep the problem tractable for the student. The surface is also illuminated by a source that subtends a small solid angle, such as the sun, at position  $(\theta_{\text{sun}}, \phi_{\text{sun}} = 0)$ . The surface is then observed from position  $(\theta_{\text{obs}}, \phi_{\text{obs}})$ , but since we set  $(\phi_{\text{sun}} = 0, \phi_{\text{sun}} = \phi_{\text{obs}} - \Delta\phi)$ , and we only consider isotropic samples, again to keep the problem tractable for the student, the observation position becomes  $(\theta_{\text{obs}}, \Delta\phi)$ . We introduce scenarios for computation where the hemispherical illumination may be simple functions of  $\theta_{\text{sky}}$ , and higher-fidelity sky radiances may be incorporated using atmospheric models, such as Spectral Sciences, Inc.’s MODTRAN® (MODerate resolution atmospheric TRANsmission)<sup>11</sup> or the AFIT’s LEEDR (Laser Environmental Effects Definition and Reference).<sup>12</sup> The “small-angle” source illumination may be a function of  $\theta_{\text{sun}}$  (as with the zenith angle of the sun due to atmospheric absorption). The observed surface is then described by various BRDF’s ranging from perfectly diffuse (i.e., Lambertian) to perfectly specular (i.e., mirror-like), and where the spherical coordinate system defined by its surface normal  $(\theta_i, \phi_i)$  may or may not align with the environmental coordinate systems  $(\theta_{\text{sky}}, \phi_{\text{sky}})$ ,  $(\theta_{\text{sun}}, \phi_{\text{sun}})$ .<sup>13</sup> All this allows the student to use the radiometry and understand the influence of each of these pieces on the observed radiance.

Note that both the self-emitted- and reflected-radiance terms of Eq. (5) are source quantities, i.e., the IR signature at zero range or as attenuated by a vacuum. In a remote-sensing scenario, apparent spectral radiance measurements, i.e., the IR signature of an object attenuated by the atmosphere over the range of the scenario, are made by a correctly calibrated instrument.

Atmospheric attenuation may then be “calibrated out” by either calibrating at range to effectively provide source measurements or by correcting apparent spectral measurements to source spectral radiance using the aforementioned atmospheric models, MODTRAN<sup>®</sup> or LEEDR. Once source spectral radiance is known, the optical characteristics of the unknown object may be determined using scene-rendering software, such as the Rochester Institute of Technology’s DIRSIG<sup>™</sup> (Digital Imaging and Remote Sensing Image Generation),<sup>14</sup> or ATA Engineering, Inc.’s SPIRITS (SPectral and In-band Radiometric Imaging of Targets and Scenes),<sup>15</sup> which uses radiometry as its basis, and illumination sources, such as the sun and sky, which are known positionally, spectrally, etc., due to time of day, temperature, and other meteorological conditions.

The IR-Technology scenario described for Fig. 1 closely aligns with the radiometric data-collection scenario we developed for our Electro-Optical-Systems-Lab course (see Fig. 2). Here, again to keep the problem tractable as a learning experience for the student, the hemispheric illumination on the unknown sample is assumed to be spatially constant (isotropic) at room temperature,  $T_{\text{Background}}$ , and the cavity blackbody and the Fourier-transform IR spectrometer (FTS) are positioned in-plane relative to the sample’s surface normal to set  $\Delta\phi = \pi$ . The cavity blackbody and FTS may be positioned at a variety of specular angles relative to the sample’s surface normal, and the sample may then be rotated to many other  $(\theta_{\text{BB}}, \theta_r)$  angle pairs away from specular to provide a rich dataset from which the optical characteristics of the unknown sample are to be determined. The cavity blackbody at temperature,  $T_{\text{BB}}$ , takes the place of the sun in the Fig. 1 scenario. The FTS is assumed to be correctly calibrated so that the measured data is the source spectral radiance, and the solid angle subtended by the FTS aperture is assumed to be small

$$\Omega_r = \frac{\pi D_{\text{FTS}}^2}{4R_{\text{Sample-FTS}}^2} = \frac{\pi(0.16 \text{ cm})^2}{4(123 \pm 0.5 \text{ cm})^2} = 1.3 \pm 0.01 \mu\text{Sr}, \quad (6)$$

where  $D_{\text{FTS}}$  is the diameter of the FTS field-of-view (FOV) aperture and  $R_{\text{Sample-FTS}}$  is the sample-to-FTS distance. Many of the concepts and processes described in the investigative-science-learning-environment (ISLE) method for education university physics students are utilized in this experiment. The student is assessed for their conceptual understanding and for their problem-solving and other scientific abilities.<sup>16</sup> Here, the student can observe that  $L_s(\Omega_r, \lambda)$  of Eq. (5) is likely unchanging across this small  $\Omega_r$ , such that  $L_s(\Omega_r, \lambda) \cong L_s(\theta_{\text{obs}}, \Delta\phi = \pi, \lambda)$  is legitimate.

With these simplifying assumptions, the self-emitted spectral radiance of Eq. (5) becomes,

$$L_e(\lambda, \theta_r, T_{\text{Room}}) = \varepsilon(\lambda, \theta_r)L_{\text{BB}}(\lambda, T_{\text{Background}}), \quad (7)$$

where  $\varepsilon(\lambda, \theta_r)$  is the spectral, directional emissivity of the sample, and  $L_{\text{BB}}(\lambda, T)$  is Planckian spectral radiance

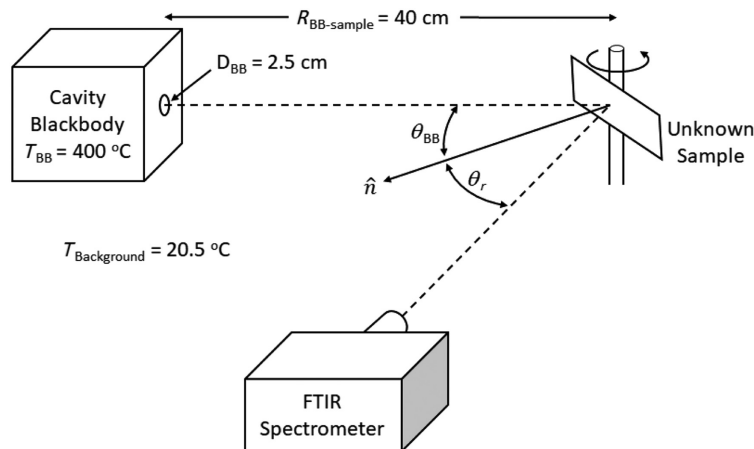


**Fig. 2** An experiment is AFIT’s Electro-Optical Systems Laboratory to provide the student with a data set from which the optical characteristics of an unknown sample are to be determined. Isotropic hemispheric illumination of the sample at  $T_{\text{Background}}$  is assumed. The cavity blackbody and the FTS are positioned in-plane relative to the sample’s surface, and they may be positioned at a variety of specular angles relative to the sample’s surface normal. The sample may then be rotated to other  $(\theta_{\text{BB}}, \theta_r)$  angles away from specular.

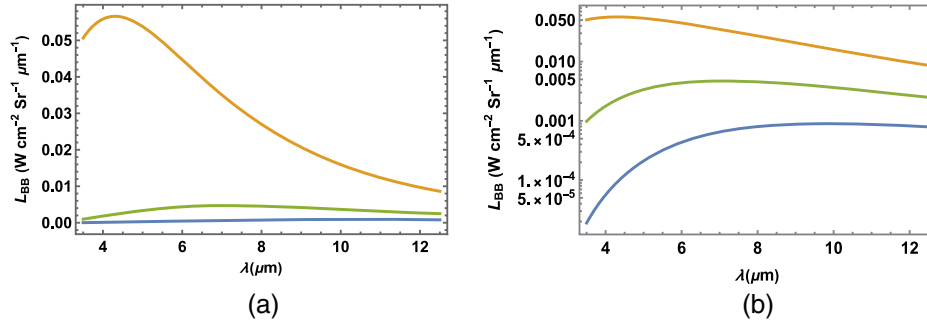


**Fig. 3** Planck's radiation law [Eq. (8)]. (a) Linear plot and (b) log-linear plot with  $T = 500^\circ\text{C}$ ,  $136^\circ\text{C}$ , and  $20.5^\circ\text{C}$  (top to bottom) and peak wavelengths at  $\lambda_{\text{peak}} = 4.3$ ,  $7.1$ , and  $9.9 \mu\text{m}$ , respectively.

$$L_{\text{BB}}(\lambda, T) = \frac{2hc^2}{\lambda^5 (e^{hc/\lambda kT} - 1)} \quad (\text{W cm}^{-2} \text{Sr}^{-1} \mu\text{m}^{-1}), \quad (8)$$

where  $h$  is the Planck constant;  $c$  is the speed of light in vacuum;  $k$  is the Boltzmann constant; and  $T$  is temperature, in this case, the sample temperature at  $T_{\text{Background}}$ . We find that the Planck spectrum is a concept that is more familiar to the physicist student in our optics program than it is to many engineering students. Although it is introduced and used in our Optical-Radiometry-and-Detection course and used extensively in our IR-Technology course, the utility of the well-known spectral content of this radiation law (Fig. 3) is still often underappreciated following those courses. This experiment has been designed to remedy that both qualitatively and quantitatively<sup>16</sup>

The reflected spectral radiance of Eq. (5) [the BRDF integral of Eq. (5)] becomes

$$L_{\text{refl}}(\lambda, \theta_r, T_{\text{BB}}, T_{\text{Background}}) = L_{\text{refl-BB}}(\lambda, \theta_r, T_{\text{BB}}) + L_{\text{refl-back}}(\lambda, \theta_r, T_{\text{Background}}), \quad (9)$$

where  $L_{\text{refl-BB}}$  is the reflected spectral radiance from the cavity blackbody at temperature,  $T_{\text{BB}}$ , and  $L_{\text{refl-back}}$  is the reflected spectral radiance from the hemispheric background at  $T_{\text{Background}}$ .  $L_{\text{refl-BB}}$  becomes

$$\begin{aligned} L_{\text{refl-BB}}(\lambda, \theta_r, T_{\text{BB}}) &= \iint_{\Omega_{\text{BB}}} \text{BRDF}(\lambda, \theta_{\text{BB}}, \theta_r, \Delta\phi = \pi) L_{\text{BB}}(\lambda, T_{\text{BB}}) \cos \theta_{\text{BB}} \sin \theta_{\text{BB}} d\theta_{\text{BB}} d\phi_{\text{BB}} \\ &\cong \text{BRDF}(\lambda, \theta_{\text{BB}}, \theta_r, \Delta\phi = \pi) L_{\text{BB}}(\lambda, T_{\text{BB}}) \cos \theta_{\text{BB}} \Omega_{\text{BB}}, \end{aligned} \quad (10)$$

where  $\Omega_{\text{BB}}$  is the solid angle subtended by the cavity blackbody aperture, which again is assumed to be small

$$\Omega_{\text{BB}} = \frac{\pi D_{\text{BB}}^2}{4R_{\text{BB-Sample}}^2} = \frac{\pi(2.5 \pm 0.1 \text{ cm})^2}{4(40 \pm 0.5 \text{ cm})^2} = 3.1 \pm 0.3 \text{ mSr}, \quad (11)$$

where  $D_{\text{BB}}$  is the diameter of the cavity blackbody aperture and  $R_{\text{BB-sample}}$  is the cavity blackbody-aperture-to-sample distance. The learning experience for the student here is that, even though  $L_{\text{BB}}(\lambda, T_{\text{BB}})$  is often assumed to be uniform across the aperture for cavity blackbodies, Eq. (10) would still need to be integrated if  $\Omega_{\text{BB}}$  were large enough that  $(\theta_{\text{BB}}, \phi_{\text{BB}})$  were changing over the integration just from the geometry. However, in this case, the student observes that even though  $\Omega_{\text{BB}}$  is not nearly as small as  $\Omega_r$ ,  $L_{\text{BB}}(\lambda, T_{\text{BB}})$  may still legitimately be considered constant across  $\Omega_{\text{BB}}$ . Furthermore, the student can observe that since  $\theta_{\text{BB}}$  is the angle of incidence of the cavity-blackbody radiation on the sample to be measured and will be varied during the experiment, it is important that  $\cos \theta_{\text{BB}}$  remains in Eq. (10) even though a “small-angle approximation” was made [similar to the discussion around Eq. (3)].

Butler says microfacet BRDF models are generally written as<sup>17</sup>

$$\text{BRDF}(\Omega_i, \Omega_r) = f_{\text{surf}}(\Omega_i, \Omega_r) + f_{\text{vol}}(\Omega_i, \Omega_r) + \frac{\rho_{\text{DDR}}(\Omega_r)}{\pi}, \quad (12)$$

where  $f_{\text{surf}}(\Omega_i, \Omega_r)$  is the surface-reflection contribution to the BRDF,  $f_{\text{vol}}(\Omega_i, \Omega_r)$  is the volumetric-scatter contribution, and  $\rho_{\text{DDR}}/\pi$  is the perfectly-diffuse- or Lambertian-scatter

contribution, where  $\rho_{\text{DDR}}(\Omega_r)$  is the directional-diffuse reflectance of the sample.<sup>18</sup> For the samples used here, we will ignore the volumetric-scatter contribution.  $L_{\text{refl-BB}}$  [Eq. (11)] then becomes

$$L_{\text{refl-BB}}(\lambda, \theta_r, T_{\text{BB}}) \cong \left[ f_{\text{surf}}(\lambda, \theta_{\text{BB}}, \theta_r, \Delta\phi = \pi) + \frac{\rho_{\text{DDR}}(\lambda, \theta_r)}{\pi} \right] L_{\text{BB}}(\lambda, T_{\text{BB}}) \cos \theta_{\text{BB}} \Omega_{\text{BB}}, \quad (13)$$

and  $L_{\text{refl-back}}$  of Eq. (9) becomes

$$\begin{aligned} L_{\text{refl-back}}(\lambda, \theta_r, T_{\text{Background}}) &= \int_{2\pi} \text{BRDF}(\lambda, \Omega_i, \Omega_r) L_i(\Omega_i, \lambda) \cos \theta_i d\Omega_i \\ &= L_{\text{BB}}(\lambda, T_{\text{Background}}) \int_{2\pi} \text{BRDF}(\lambda, \Omega_i, \Omega_r) \cos \theta_i d\Omega_i \\ &= L_{\text{BB}}(\lambda, T_{\text{Background}}) \rho_{\text{HDR}}(\lambda, \theta_r), \end{aligned} \quad (14)$$

where again the hemispheric illumination on the unknown sample is assumed to be spatially constant (isotropic) at  $T_{\text{Background}}$ , and where  $\rho_{\text{HDR}}(\lambda, \Omega_r)$  is the hemispherical-directional reflectance<sup>18</sup> and is  $\rho_{\text{HDR}}(\lambda, \theta_r)$  for the isotropic reflectors used here. Here, for the purpose of student learning, integrating  $L_i(\Omega_i, \lambda)$  over  $\Omega_i$  with high fidelity is not practical. However, they can observe just how appropriate this isotropic approximation is or is not with available thermal cameras. Furthermore, Eq. (14) provides them with a useful application of the relationship between the BRDF and  $\rho_{\text{HDR}}$ .

The spectral radiance leaving the surface in Eq. (5) becomes the measured spectral radiance here

$$\begin{aligned} L_{\text{meas}}(\lambda, \theta_{\text{BB}}, \theta_r, T_{\text{Background}}, T_{\text{BB}}, \Omega_{\text{BB}}) &= [1 - \rho_{\text{HDR}}(\lambda, \theta_r)] L_{\text{BB}}(\lambda, T_{\text{Background}}) \\ &+ \left[ f_{\text{surf}}(\lambda, \theta_{\text{BB}}, \theta_r, \Delta\phi = \pi) + \frac{\rho_{\text{DDR}}(\lambda, \theta_r)}{\pi} \right] L_{\text{BB}}(\lambda, T_{\text{BB}}) \cos \theta_{\text{BB}} \Omega_{\text{BB}} \\ &+ L_{\text{BB}}(\lambda, T_{\text{Background}}) \rho_{\text{HDR}}(\lambda, \theta_r) \\ &= L_{\text{BB}}(\lambda, T_{\text{Background}}) + \left[ f_{\text{surf}}(\lambda, \theta_{\text{BB}}, \theta_r, \Delta\phi = \pi) + \frac{\rho_{\text{DDR}}(\lambda, \theta_r)}{\pi} \right] L_{\text{BB}}(\lambda, T_{\text{BB}}) \cos \theta_{\text{BB}} \Omega_{\text{BB}}, \end{aligned} \quad (15)$$

since the directional form of Kirchoff's law for opaque materials,  $\varepsilon(\lambda, \theta_r) = 1 - \rho_{\text{HDR}}(\lambda, \theta_r)$ , holds because of the quantum-mechanical principal of time-invariance, which certainly applies to these samples.<sup>19</sup>

With this background, Sec. 2 will cover the methods of instrument calibration, data collection and analysis, and a description of the two samples chosen for use in this experiment in our Electro-Optical-Systems-Lab course. Section 3 will show example measurement results and analyses and demonstrate through this experiment what radiometry can reveal to the student about a measured sample's characteristics. Section 4 concludes the paper.

## 2 Methods

Prior to the start of data collection for this experiment, the student is encouraged to explore the possibilities of Eq. (15) to understand the spectral data they will collect and how to begin to interpret/analyze it. Representing an empirically observed pattern mathematically is one of the scientific abilities the ISLE methodology encourages. As will be shown in Sec. 3, Eq. (15) fully represents the observed trends, and elicits analyses of just how well it agrees with the data.<sup>20</sup>

Figure 4 shows a case where the sample is spectrally constant and perfectly diffuse (Lambertian), so  $f_{\text{surf}}(\theta_{\text{BB}}, \theta_r, \Delta\phi = \pi) = 0$  may be set and  $\rho_{\text{DDR}}(\theta_r)$  essentially becomes  $\rho_{\text{HDR}}(\theta_r)$ , with  $0 \leq \rho_{\text{HDR}} \leq 1$ ; it uses  $T_{\text{Background}} = 20.5^\circ\text{C}$  and  $\theta_{\text{BB}} = 45^\circ$ . Figure 4(a) uses  $T_{\text{BB}} = 400^\circ\text{C}$  and shows four curves, from bottom to top, a Planckian at  $T_{\text{Background}}$  and three plots of Eq. (15) with  $\rho_{\text{DDR}} = 0, 0.5, \text{ and } 1$ , respectively. It tells the student that if they collect

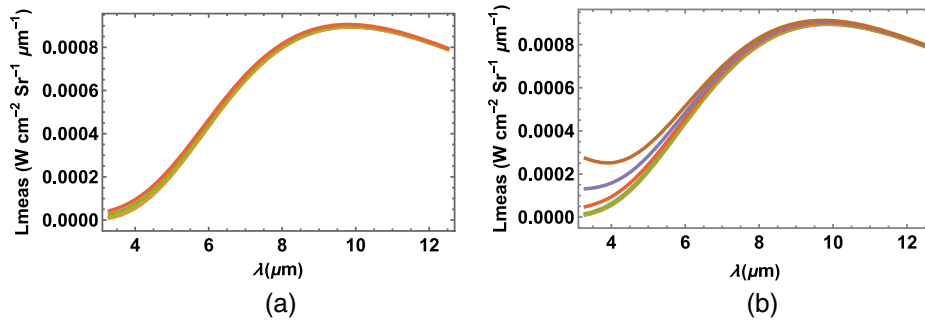


**Fig. 4** Plots of Eq. (15) for a diffuse (Lambertian) sample.  $f_{\text{surf}}(\theta_{\text{BB}}, \theta_r, \Delta\phi = \pi) = 0$ ,  $T_{\text{Background}} = 20.5^\circ\text{C}$ , and  $\theta_{\text{BB}} = 45^\circ$ . In both plots, the lowest curve is a Planckian at  $T_{\text{Background}}$ . (a)  $T_{\text{BB}} = 400^\circ\text{C}$  and from the bottom,  $\rho_{\text{DDR}} = 0, 0.5$ , and  $1$ , respectively. (b)  $\rho_{\text{DDR}} = 0.5$  and from the bottom,  $T_{\text{BB}} = 100^\circ\text{C}, 300^\circ\text{C}, 500^\circ\text{C}, 700^\circ\text{C}$ , and  $900^\circ\text{C}$ , respectively.

data that appears Planckian at  $T_{\text{Background}}$ , they are likely measuring a diffuse sample and should begin data analysis appropriately. Figure 4(b) uses  $\rho_{\text{DDR}} = 0.5$  and shows six curves, again from bottom to top, a Planckian at  $T_{\text{Background}}$  and five curves with  $T_{\text{BB}} = 100, 300, 500, 700$ , and  $900^\circ\text{C}$ , respectively. It tells the student that for diffuse samples, the “small angle” illumination must be very bright before it pulls the spectrum away from that of the background Planckian, and then that that difference is largest at shorter wavelengths where the Planckian of the hotter source peaks.

Figure 5 is a second example, where the sample is again spectrally constant but now perfectly specular.  $\rho_{\text{DDR}}(\theta_r) = 0$  may be set in Eq. (15) and the specular BRDF,  $f_{\text{surf}}(\theta_{\text{BB}}, \theta_r, \Delta\phi = \pi)$ , may be studied. It again uses  $T_{\text{Background}} = 20.5^\circ\text{C}$ ,  $T_{\text{BB}} = 400^\circ\text{C}$ , and  $\theta_{\text{BB}} = 45^\circ$ . Figure 5(a) shows six plots, again from bottom to top, a Planckian at  $T_{\text{Background}}$  and five plots of Eq. (15) with  $f_{\text{surf}}(\theta_{\text{BB}}, \theta_r, \Delta\phi = \pi) = 5, 10, 20, 30$ , and  $40 \text{ Sr}^{-1}$ , respectively. It tells the student that the more the spectrum moves away from the  $T_{\text{Background}}$  Planckian, the more specular the sample likely is. Figure 5(b) shows four plots, this time from top to bottom, a Planckian at  $T_{\text{BB}}$  and three plots of Eq. (15) with  $f_{\text{surf}}(\theta_{\text{BB}}, \theta_r, \Delta\phi = \pi) = 300, 200$ , and  $100 \text{ Sr}^{-1}$ , respectively. It tells the student they are essentially observing the virtual image of the “small-angle source” through a specular “mirror,” and as the sample reflectance increases, the  $T_{\text{BB}}$  Planckian dominates the  $T_{\text{Background}}$  Planckian, as expected since  $T_{\text{BB}} \gg T_{\text{Background}}$ .

Again, referring to the ISLE methodology, the concept is that the best learning experience for the student is that they design experiments for themselves to find phenomenological patterns in the data, devise hypotheses to explain the phenomena, design experiments to test their hypotheses, and even rule out hypotheses based on those experimental results.<sup>16</sup> Although that aspect of the process is not what is presented here, it is a paradigm we try to follow in our

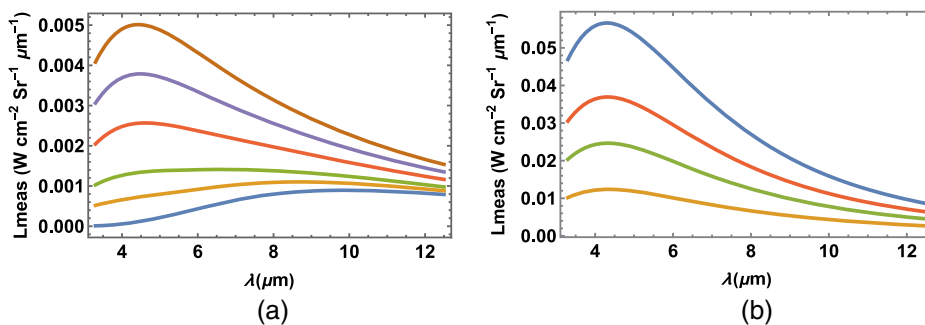


**Fig. 5** Plots of Eq. (15) for a perfectly specular sample.  $T_{\text{Background}} = 20.5^\circ\text{C}$ ,  $T_{\text{BB}} = 400^\circ\text{C}$  and  $\theta_{\text{BB}} = 45^\circ$ . In both plots, the lowest curve is a Planckian at  $T_{\text{Background}}$ . (a) Bottom-most plot is a Planckian at  $T_{\text{Background}}$ . Moving upward,  $f_{\text{surf}}(\theta_{\text{BB}}, \theta_r, \Delta\phi = \pi) = 5, 10, 20, 30$  and  $40 \text{ Sr}^{-1}$ , respectively. (b) Top-most plot is a Planckian at  $T_{\text{BB}}$ . Moving downward,  $f_{\text{surf}}(\lambda, \theta_{\text{BB}}, \theta_r, \Delta\phi = \pi) = 300, 200$ , and  $100 \text{ Sr}^{-1}$  respectively.

Electro-Optical-Systems-Lab course since this course is considered preparation for the student's upcoming thesis/dissertation experience. e.g., one student lab group proposed doing this radiometry experiment with an imager rather than a spectrometer. As shown in Figs. 4 and 5, the useful patterns in this experiment are spectral. The strength of an imager is that it provides spatial information, of which there is very little useful in this experiment, generally at the expense of spectral information, which has been integrated out over the spectral band of the detector. This may be considered as a simplified version of the well-known temperature-emissivity-separation problem in remote sensing.<sup>21</sup> With some work, Eq. (13) could be in a form like Eqs. (7) and (14), such that its spectral integral is  $\int_{\Delta\lambda} \rho_{\text{eff}}(\lambda) L_{\text{BB}}(\lambda, T) d\lambda$ . Then, even when the emissivity or reflectance are constant, such as the cases shown in Fig. 6 for the mid-wave IR (MWIR, 3.3 – 5.6  $\mu\text{m}$  here) and long-wave IR (LWIR, 5.6 – 12.5  $\mu\text{m}$  here), separate identification of  $\rho_{\text{eff}}$  and  $T$  is not possible. These students limited their success by “choosing” to integrate out important information. Although every student in our Electro-Optical-Systems-Lab course does not have the opportunity to propose and rule out hypotheses such as this, just in the interest of time in a 10-week course, the redacted laboratory report from this failed experiment is made available to the students working the spectral version for their information.

In our Electro-Optical-Systems-Lab course, one of the instruments used is a Bomem MR 154 FTS with a liquid-nitrogen ( $\text{LN}_2$ )-cooled mercury-cadmium-telluride (MCT) photodiode for the 800 to 1800- $\text{cm}^{-1}$  (5.6 – 12.5- $\mu\text{m}$ ) band and an  $\text{LN}_2$ -cooled indium-antimonide photodiode for the 1800 to 3000  $\text{cm}^{-1}$  (3.3 to 5.6- $\mu\text{m}$ ) band. The dataset presented henceforth was collected using a medium-angle telescope, and the detectors were calibrated for spectral radiance ( $\text{W cm}^{-2} \text{Sr}^{-1} \text{cm}$ ) with 1.93- $\text{cm}^{-1}$  resolution, smoothed to 13.5- $\text{cm}^{-1}$  resolution, at the 123-cm collection distance using an Electro-Optical Industries, Inc. wide-area 2" blackbody for temperatures of 20 to 200°C and an Electro-Optical Industries, Inc. cavity blackbody for temperatures of 200 to 410°C, and converted to ( $\text{W cm}^{-2} \text{Sr}^{-1} \mu\text{m}^{-1}$ ) spectral radiance in post-processing. Both blackbody apertures overfilled the FTS FOV.

The reflectance samples used were polished aluminum (Al), henceforth referred to as the “specular” sample, and flamed-sprayed Al, henceforth referred to as the “diffuse” sample, both with gold (Au) deposited on them (Fig. 7). These are great initial samples for the student because they are near the extremes of specular/diffuse scatter that the student explored using Eq. (15); the specular sample is very mirror-like and the diffuse sample approaches Lambertian, especially at near-normal incidence angles. The Au deposition makes their reflectance rather constant spectrally, again, simplifying the application of Eq. (15) as a starting point by removing the spectral dependence of the reflectance terms.

To quantify these samples' characteristics, they were measured using a Surface Optics Corp. SOC-100 Hemispherical Directional Reflectometer<sup>22</sup> with a Nicolet iS50 FT-IR FTS with a DTGS pyroelectric detector over the spectral band studied here. The  $\rho_{\text{HDR}}(\lambda, \theta_r)$ ,  $\rho_{\text{DDR}}(\lambda, \theta_r)$  and spectral specular-directional reflectance,  $\rho_{\text{SDR}}(\lambda, \theta_r)$ , are shown in Fig. 8. Details are included in the figure caption.

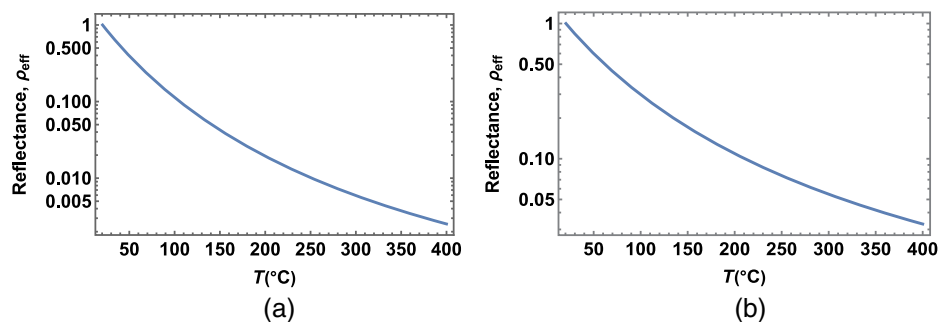


**Fig. 6** Constant band-integrated radiance,  $\rho_{\text{eff}} \int_{\Delta\lambda} L_{\text{BB}}(\lambda, T) d\lambda$ , makes solution of  $(\rho_{\text{eff}}, T)$  nonunique. (a) MWIR, 3.3 – 5.6  $\mu\text{m}$ ,  $L(\rho_{\text{eff}}, T) = 310 \mu\text{W cm}^{-2} \text{Sr}^{-1}$ . (b) LWIR, 5.6 to 12.5  $\mu\text{m}$ ,  $L(\rho_{\text{eff}}, T) = 5.3 \text{ mW cm}^{-2} \text{Sr}^{-1}$ .

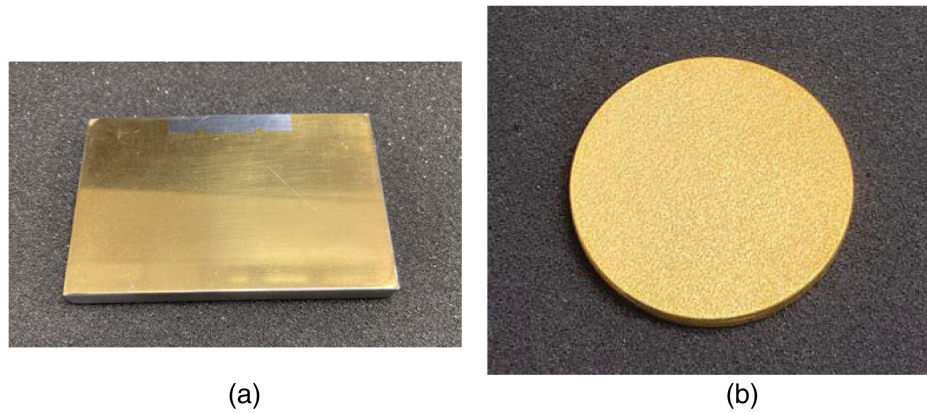


**Fig. 7** Reflectance samples used. (a) Polished Al, aka the “specular” sample, and (b) flamed-sprayed Al, aka the “diffuse” sample, both with Au deposited on them.

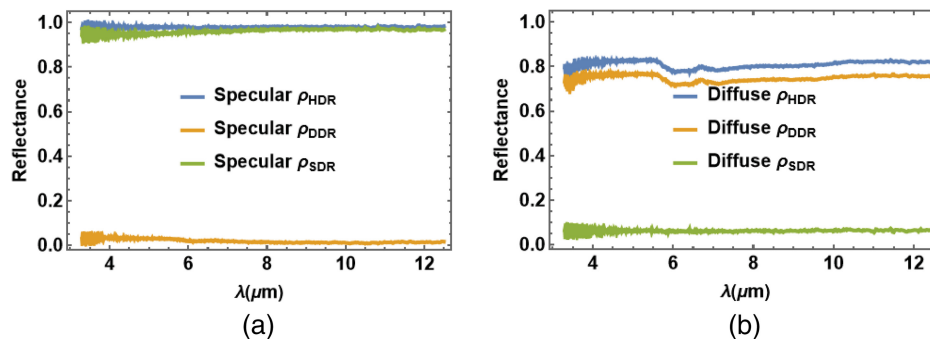


**Fig. 8** At  $40 \text{ deg} \leq \theta_r \leq 50 \text{ deg}$ , (a) for the polished sample,  $\rho_{\text{HDR}} = 0.98 \pm 0.004$ ,  $\rho_{\text{DDR}} = 0.024 \pm 0.008$ , and  $\rho_{\text{SDR}} = 0.95 \pm 0.01$ , across the 3.3- to 12.5- $\mu\text{m}$  band, and (b) for the flame-sprayed sample,  $\rho_{\text{HDR}} = 0.81 \pm 0.02$ ,  $\rho_{\text{DDR}} = 0.75 \pm 0.02$ , and  $\rho_{\text{SDR}} = 0.06 \pm 0.006$ , across this band.

### 3 Results and Analysis

Data should be collected by the student at several initial  $\theta_{\text{BB}} = \theta_r$  specular angles (again, at any one of which, the sample may then be rotated away from specular) to give the student a rich data set to study how the angle-dependent reflectance impacts the radiometry. Two scientific abilities the ISLE methodology seeks to develop in the student are designing an experiment that yields interesting patterns for the investigation of some phenomenon and identifying those patterns in the data collected.<sup>20</sup> The data are excellent for that.

#### 3.1 Specular Sample

Data from initial specular angles of  $\theta_{\text{BB}} = \theta_r = 11^\circ, 21^\circ, 30^\circ$ , and  $62^\circ$  are used here and the sample was rotated by  $\pm 1^\circ, 2^\circ$ , and  $3^\circ$  in each case. The virtual image of the cavity blackbody aperture viewed through the sample “mirror” subtends a planar angle of

$$\theta = \frac{D_{\text{BB}}}{R_{\text{BB-FTS}}} = \frac{2.5 \text{ cm}}{(40 + 123) \text{ cm}} = 15 \text{ mrad} = 0.88^\circ, \quad (16)$$

so little interesting data change was expected beyond the  $\pm 3^\circ$ . Figure 9 shows examples of the data collected. Figure 9(a) is a measurement at  $\theta_{\text{BB}} = \theta_r = 21^\circ$  and (b) is off specular at ( $\theta_{\text{BB}} = 20^\circ, \theta_r = 22^\circ$ ). Note the noise in the spectra; between the low responsivity of the MCT detector and the low signal in the water-vapor band of  $\sim 5.6$  to  $8 \mu\text{m}$ , this was not uncommon, and at times, made curve-fitting difficult. Although the student can see this is a mirror-like sample as they set up the experiment, the assumption is that even without this knowledge, they should recognize from their own preparation leading to plots like those of Figs. 4 and 5 and the behavior of this data that this is a specular sample and proceed with analysis accordingly.

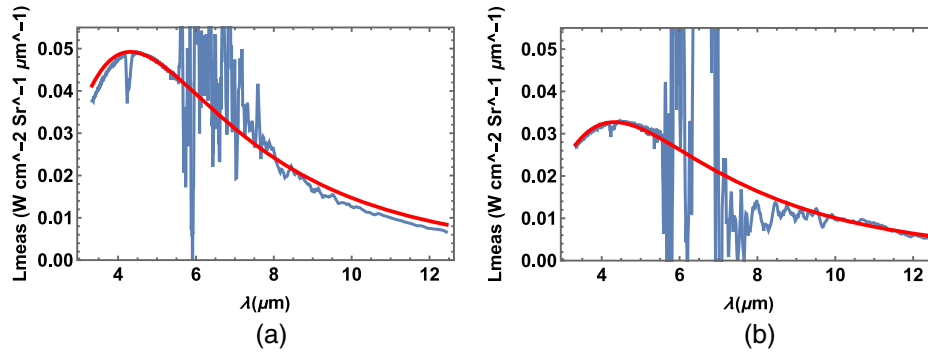


**Fig. 9** (Blue) Measurement data for specular sample and (red) best fit of Eq. (15).  $T_{\text{Background}} = 20.5 \pm 0.5^\circ\text{C}$  and  $T_{\text{BB}} = 400^\circ\text{C}$ .  $\rho_{\text{DDR}}(\theta_r) = 0$  and  $f_{\text{surf}}(\theta_{\text{BB}}, \theta_r, \Delta\phi = \pi)$  is the fitting parameter are set for the fits. (a)  $\theta_{\text{BB}} = \theta_r = 21$  deg and  $f_{\text{surf}} = 303 \text{ Sr}^{-1}$ . (b)  $\theta_{\text{BB}} = 20$  deg and  $\theta_r = 22$  deg and  $f_{\text{surf}} = 200 \text{ Sr}^{-1}$ .

The red lines in each plot of Fig. 9 are the best fit of Eq. (15) to the data, using  $T_{\text{Background}} = 20.5^\circ\text{C}$  and  $T_{\text{BB}} = 400^\circ\text{C}$ , and making the assumption that illumination sources are reasonably well known, as they are in many remote-sensing scenarios and that the sample is at  $T_{\text{Background}}$  here. (Note that  $T_{\text{Background}} = 20.5 \pm 0.5^\circ\text{C}$  across all the data-collection and instrument-calibration days, and the Electro-Optical Industries, Inc. cavity blackbody was set to  $T_{\text{BB}} = 400^\circ\text{C}$ .) Knowledge of  $(\theta_{\text{BB}}, \theta_r)$  is also assumed, again, as might be true in many remote-sensing scenarios. Following the argument from Fig. 5,  $\rho_{\text{DDR}}(\lambda, \theta_r) = 0$  is set (which works out well here since  $\text{DDR} = 0.024 \pm 0.008$  for the specular sample), leaving  $f_{\text{surf}}(\theta_{\text{BB}}, \theta_r, \Delta\phi = \pi)$  as the only fitting parameter.

Table 1 shows results of all the  $f_{\text{surf}}$  fits. The rows are the incident angles,  $\theta_{\text{BB}}$ , and the columns are the reflectance (observation) angles,  $\theta_r$ , making the table diagonal to the specular case,  $\theta_{\text{BB}} = \theta_r$ . Moving down the diagonal of the table from upper left to lower right, reflectance increases as incident angle,  $\theta_{\text{BB}}$ , increases, as expected. Looking at the off-specular results for any of the three-element specular-datasets, reflectance is always greater on the forward-scatter side of specular ( $\theta_r > \theta_{\text{BB}}$ ) than it is on the back-scatter side ( $\theta_{\text{BB}} > \theta_r$ ), again as expected. The

**Table 1** Results of fitting  $f_{\text{surf}}(\theta_{\text{BB}}, \theta_r, \Delta\phi = \pi)$  (units of  $\text{Sr}^{-1}$ ) of Eq. (14) to the specular-sample data.

	$\theta_r(\text{deg})$											
$\theta_{\text{BB}}(\text{deg})$	10	11	12	20	21	22	29	30	31	61	62	63
10			235									
11		261										
12	122											
20						200						
21					303							
22			160									
29									195			
30								315				
31							245					
61												300
62											625	
63										410		

ISLE methodology also suggests the adequate experiment for developing the scientific ability of identifying relevant patterns in data allows those trends to be described in words.<sup>20</sup> This does that. These are concepts that were introduced to the student in our IR-Technology course but are likely not retained without sufficient repetition/use. Although this experiment is well designed to do that, we said earlier that the FTS is assumed to be well aligned/well calibrated, and in our Electro-Optical-Systems-Lab course, this is not always the case. Hence, the collected data may differ from the examples shown here and lead to confusion in the analyses. This can be a good thing! The course description says this lab introduces laboratory techniques for the measurement of radiometric quantities. The synergy between data collection and theory is more important than ever with modern computational power.<sup>23</sup> Encouragement by the instructor to double check alignment/calibration is not only part of learning the laboratory techniques but is also an introduction to that synergy. Back to the Table 1 data, the spectral shape of the measured data for angles greater than  $\pm 1^\circ$  off specular, as well as the noise in that data, prohibited good fitting results for those angles.

### 3.2 Diffuse Sample

For the diffuse sample, initial specular angles of  $\theta_{\text{BB}} = \theta_r = 11^\circ, 21^\circ, 30^\circ, 45^\circ,$  and  $62^\circ$  were again used, but the sample was rotated away from specular by much larger angles,  $\leq |\pm 33^\circ|$ . Figure 10 shows examples of the data collected. Figure 10(a) is a measurement at  $(\theta_{\text{BB}} = 23^\circ, \theta_r = 19^\circ)$ , (b) at  $(\theta_{\text{BB}} = 53^\circ, \theta_r = 7^\circ)$ , and (c) at  $(\theta_{\text{BB}} = \theta_r = 45^\circ)$ . Again, although the student can see this is a rough-surfaced sample as they set up the experiment, the assumption is that even without this knowledge, they should recognize from their own preparation leading to plots like those of Figs. 4 and 5 and the behavior of this data that this is a diffuse sample and proceed with analysis accordingly.

The green lines in each plot of Fig. 10 are the again best fits of Eq. (15) to the data, using  $T_{\text{Background}} = 20.5^\circ\text{C}$  and  $T_{\text{BB}} = 400^\circ\text{C}$ , and again making the assumptions that the sample is at  $T_{\text{Background}}$  and that  $\theta_{\text{BB}}$  and  $\theta_r$  are known. The red lines are Planckians at  $T_{\text{Background}}$ . Following the argument from Fig. 4,  $f_{\text{surf}}(\theta_{\text{BB}}, \theta_r, \Delta\phi = \pi) = 0$  should be set, leaving  $\rho_{\text{DDR}}(\theta_r)$  as the fitting parameter. This works well as an initial guess, however, as will be shown by the lower plot of Fig. 10, this sample is diffuse but not Lambertian, so a simultaneous fit of  $f_{\text{surf}}$  and  $\rho_{\text{DDR}}$  in Eq. (15) is a better choice. Assuming the student can do, or at least follow, the argument of Eqs. (12)–(15), this is a very reasonable and computationally tractable stretch. Note that the fitting constraint used here is  $\rho_{\text{DDR}} \leq 1$ , which is obviously physical.

Figure 10(a) shows the  $(\theta_{\text{BB}} = 23^\circ, \theta_r = 19^\circ)$  case, where the fit did produce  $f_{\text{surf}} = 0$ , with  $\rho_{\text{DDR}} = 0.82$  (recall that the measured DDR =  $0.75 \pm 0.02$  for the diffuse sample). As in Fig. 4(a), this data resembles the  $T_{\text{Background}}$  Planckian but lies above it, so  $\rho_{\text{DDR}} > 0$  gave a good fit. Figure 10(b) shows the  $(\theta_{\text{BB}} = 73^\circ, \theta_r = 7^\circ)$  case; like much of the data well away from the specular angle, the best fit to the data was  $(f_{\text{surf}} = 0, \rho_{\text{DDR}} = 0)$ , indicating there is little appreciable contribution from the cavity blackbody and the best fit to the data is a  $T_{\text{Background}}$  Planckian. Figure 10(c) shows the  $(\theta_{\text{BB}} = 45^\circ, \theta_r = 45^\circ)$  case, where the fit produced

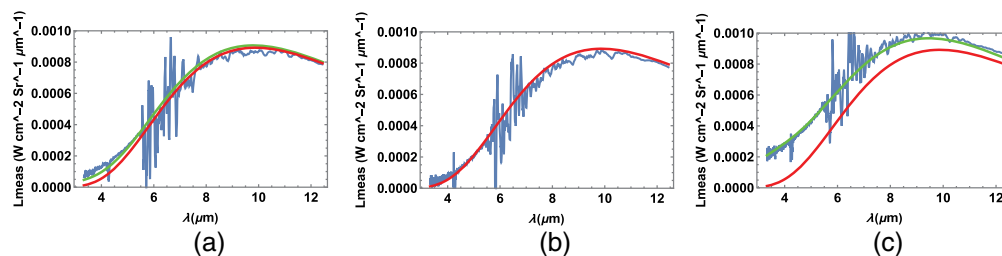


**Fig. 10** (Blue) Measurement data for diffuse sample. The green lines are the best fits of Eq. (15) to the data, using  $T_{\text{Background}} = 20.5^\circ\text{C}$  and  $T_{\text{BB}} = 400^\circ\text{C}$ , and that the sample is at  $T_{\text{Background}}$ . The red lines are Planckians at  $T_{\text{Background}}$ . (a)  $(\theta_{\text{BB}} = 23 \text{ deg}, \theta_r = 19 \text{ deg})$ , best-fit results ( $f_{\text{surf}} = 0, \rho_{\text{DDR}} = 0.82$ ). (b)  $(\theta_{\text{BB}} = 73 \text{ deg}, \theta_r = 7 \text{ deg})$ , best-fit results ( $f_{\text{surf}} = 0, \rho_{\text{DDR}} = 0$ ), (best fit is a Planckian at  $T_{\text{Background}}$ ). (c)  $(\theta_{\text{BB}} = 45 \text{ deg}, \theta_r = 45 \text{ deg})$ , best-fit results ( $f_{\text{surf}} = 1.6 \text{ Sr}^{-1}, \rho_{\text{DDR}} \sim 1$ ), (the  $f_{\text{surf}}$  component models the forward scattering of this non-Lambertian sample).

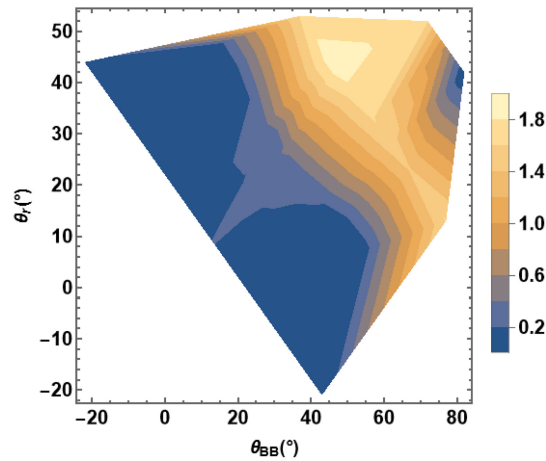


**Fig. 11** Results of fitting  $\text{BRDF}(\theta_{\text{BB}}, \theta_r) = f_{\text{surf}}(\theta_{\text{BB}}, \theta_r) + \rho_{\text{DDR}}(\theta_{\text{BB}}, \theta_r)/\pi$  (units of  $\text{Sr}^{-1}$ ) of Eq. (15) to the diffuse-sample data.

( $f_{\text{surf}} = 1.6 \text{ Sr}^{-1}$ ,  $\rho_{\text{DDR}} \sim 1$ ).  $\rho_{\text{DDR}}$  being constrained to 1 was the case for many of the  $30^\circ \leq \theta_{\text{BB}} \leq 62^\circ$  data due to the forward-scattering nature of this non-Lambertian sample. Referencing Fig. 4, such data cannot be modeled by diffuse scatter alone and requires the  $f_{\text{surf}}$  component, but again, this is still a tractable stretch for the student. Recall that the measured  $\text{SDR} = 0.06 \pm 0.006$  for the diffuse sample; it is difficult to draw the link between  $\text{BRDF}(\Omega_i, \Omega_r)$  and  $\rho_{\text{HDR}}(\Omega_r)$  or  $\rho_{\text{SDR}}(\Omega_r)$  without much higher resolution  $\Omega_r$  measurements.

Figure 11 shows results of all the  $(f_{\text{surf}}, \rho_{\text{DDR}})$  fitting, shown as  $\text{BRDF}(\theta_{\text{BB}}, \theta_r) = f_{\text{surf}}(\theta_{\text{BB}}, \theta_r) + \rho_{\text{DDR}}(\theta_{\text{BB}}, \theta_r)/\pi$ , and represents an estimated (and reasonable) BRDF plot for this diffuse sample. The specular ( $\theta_{\text{BB}} = \theta_r$ ) diagonal runs lower left to upper right but is not very prominent in a diffuse sample. The BRDF increases with increasing incident angle,  $\theta_{\text{BB}}$ , as expected for a non-Lambertian sample, and increases on the upper left of the ( $\theta_{\text{BB}} = \theta_r$ ) diagonal compared to the lower right since the BRDF is typically greater on the forward-scatter side of specular than it is on the backscatter side. Again, these are concepts that were introduced to the student in our IR-Technology course but are likely not retained without sufficient repetition/use. And again, the ISLE methodology suggests the adequate experiment for developing the scientific ability of identifying relevant patterns in data also allows those trends to be described in words.<sup>20</sup> This experiment is well designed to do that.

### 3.3 Findings

This BRDF experiment in our Electro-Optical-Systems-Lab course was devised to help the student develop a better understanding of radiometry and radiometric instrumentation, and how they can be used to gain an understanding of a material's optical properties in a remote-sensing scenario, which is another concept introduced in our IR-Technology course. As an initial, tractable problem for the student, it allows them success in the differentiation between a specular sample and a diffuse one, and after that differentiation, success in their initial quantification of a sample's reflectance properties of  $f_{\text{surf}}(\theta_{\text{BB}}, \theta_r, \Delta\phi = \pi)$  and  $\rho_{\text{DDR}}(\theta_r)$ . It provides useful experience upon which much more difficult remote-sensing analyses may be built. Finally, all students present their findings and procedures to the rest of the class in our Electro-Optical-Systems-Lab course, another experience encouraged by the ISLE methodology.<sup>20</sup>

## 4 Conclusions

AFIT offers a three-course optics sequence to educate students in radiometry and radiometric instrumentation, and their applications. This paper described a BRDF experiment developed for our Electro-Optical-Systems-Lab course to help students gain a better understanding of radiometry and radiometric instrumentation. The groundwork for the BRDF and its analysis is laid in

our earlier (IR)-Technology course. This experiment uses a Fourier-transform IR spectrometer (FTS), a cavity blackbody, and samples whose reflectance properties range from specular to diffuse. We find this experiment to be useful in helping the student not only to understand radiometry and radiometric instrumentation but also how they can be used to gain an understanding of a material's optical properties in a remote-sensing scenario. It also provides success in an initial radiometry experience upon which more difficult remote-sensing analyses may be built.

Limitations of the initial experiment described here include sample measurements being limited to in-plane, i.e., both illumination source and detector were positioned in-plane relative to the sample's surface normal. The generalization of this obviously includes out-of-plane measurements, but those results are likely not much different than the off-specular results reported here. Another limitation is that the reflectance properties of the initial samples presented here were limited to the simple cases of being either very specular or very diffuse. Furthermore, these samples were gold-coated metal, which is rather constant spectrally in the IR region studied here. Generalization of these includes the extension to samples whose specularity is somewhere between these two extremes (as most real-world materials are) and are dielectric, such that their reflectance might have some spectral content and volume scatter would complicate the BRDF model required for their analyses.

Even with these simplifying constraints, we believe this is a good radiometry-laboratory experiment to advance the student's optics education.

---

## Disclosures

Opinions, conclusions, and recommendations expressed or implied within are solely those of the author and do not necessarily represent the views of the Air Force Institute of Technology, Air University, the United States Air Force, the Department of Defense, or any other US Government agency. Cleared for public release: distribution unlimited.

## Code and Data Availability

The data that support the findings of this article were collected at the Air Force Institute of Technology and are not publicly available. They can be requested from the author at michael.marciniak@us.af.mil.

## Acknowledgments

I would like to thank AFIT Department of Engineering Physics technicians, Mr. Greg Smith and Mr. Ben Doane, for their assistance in setting up this experiment and calibrating the instruments. This work is part of AFIT's Electro-Optical Systems Lab course, and therefore, is not part of any sponsored research.

## References

1. Graduate School of Engineering and Management, Air Force Institute of Technology, <https://www.afit.edu/EN/> (accessed 14 November 2023).
2. W. L. Wolfe and G. J. Zissis, Eds., *The Infrared Handbook*, Infrared Information and Analysis Center, Ann Arbor, Michigan (2001).
3. E. Wolf, "Coherence and radiometry," *J. Opt. Soc. Am.* **68**(1), 6–17 (1978).
4. Air Force Institute of Technology, "Graduate School Catalog 2022-2023," <https://www.afit.edu/docs/22-23%20GSEM%20Catalog.pdf> (accessed 14 November 2023).
5. F. Nicodemus, "Directional reflectance and emissivity of an opaque surface," *Appl. Opt.* **4**(7), 767–775 (1965).
6. J. M. Palmer, *The Art of Radiometry*, SPIE Press, Bellingham, WA (2010).
7. J.-J. Grefft and M. Nieto-Vesperinas, "Field theory for generalized bidirectional reflectivity: derivation of Helmholtz's reciprocity principle and Kirchhoff's law," *J. Opt. Soc. Am. A* **15**(10), 2735–2744 (1998).
8. D.S. Immel et al., "A radiosity method for non-diffuse environments," *Comp. Graph.* **20**(4), 133–142 (1986).
9. J.T. Kajiya, "The rendering equation," *Comp. Graph.* **20**(4), 143–150 (1986).
10. G. Schaepman-Strub et al., "Reflectance quantities in optical remote sensing—definitions and case studies," *Remote Sens. Environ.* **103**, 27–42 (2006).
11. MODTRAN<sup>®</sup>, Spectral Sciences, Inc., <http://modtran.spectral.com/> (accessed 15 November 2023).
12. Laser Environmental Effects Definition and Reference (LEEDR), Center for Directed Energy, Air Force Institute of Technology, <https://www.afit.edu/CDE/page.cfm?page=329> (accessed 22 November 2023).

13. D. M. Stoyanov, M. A. Marciniak, and J. N. Meola, "Comparative study of spectral diffuse-only and diffuse-specular radiative transfer models and field-collected data in the LWIR," *Proc. SPIE* **9611**, 96110H (2015).
14. DIRSIG™, Chester F. Carlson Center for Imaging Science, Rochester Institute of Technology, <https://dirsig.cis.rit.edu/> (accessed 15 November 2023).
15. SPIRITS, ATA Engineering, Inc., <https://www.ata-e.com/software/software-we-use/spirits/> (accessed 15 November 2023).
16. E. Etkina and A. Van Heuvelen, "Investigative science learning environment - a science process approach to learning physics," in *Research-Based Reform of University Physics*, E. F. Redish and P. J. Cooney, Eds., Vol. 1, American Association of Physics Teachers, College Park, Maryland (2007).
17. S. D. Butler and M. A. Marciniak, "Robust categorization of microfacet BRDF models to enable flexible application-specific BRDF adaptation," *Proc. SPIE* **9205**, 920506 (2014).
18. G. J. Zissis, Ed., *The IR & EO Systems Handbook*, Vol. 1, Sources of Radiation, Infrared Information and Analysis Center, Ann Arbor, Michigan (1993).
19. W. C. Snyder et al., "Thermodynamic constraints on reflectance reciprocity and Kirchhoff's law," *Appl. Opt.* **37**(16), 3464 (1998).
20. E. Etkina, "When learning physics mirrors doing physics," *Phys. Today* **76**(10), 26–32 (2023).
21. C. C. Borel and R. F. Tuttle, "Recent advances in temperature-emissivity separation algorithms," in *Aerosp. Conf.*, Big Sky, MT, USA, pp. 1–14 (2011).
22. SOC-100 HDR Hemispherical Directional Reflectometer, Surface Optics Corp., <https://surfaceoptics.com/products/reflectometers-emissometers/soc-100-hdr/> (accessed 15 November 2023).
23. F. Darema, "Dynamic data driven applications systems: a new paradigm for application simulations and measurements," *Lect. Notes Comput. Sci.* **3038**, 662–669 (2004).

**Michael A. Marciniak** is a professor at the Air Force Institute of Technology. He received his BS degree in mathematics from St. Joseph's College, IN, BSEE from the University of Missouri-Columbia and MSEE and PhD degrees from AFIT. His current research interests include bidirectional scatter distributions and scatterometry of optical metasurfaces. He has advised 14 PhD dissertations and 57 MS theses and published over 50 refereed and 85 other technical papers. He is a senior member of SPIE.